Study of the fracture behaviour in hybrid fibers reinforced thermoplastic laminates: Influence of temperature and initial notch orientation

Benoît Vieille, Juan Daniel Pujols Gonzalez, Christophe Bouvet

Study of the fracture behaviour in hybrid fibers reinforced thermoplastic laminates: Influence of temperature and initial notch orientation

B. Vieille *, J.-D. Pujols-Gonzalez, C. Bouvet

Groupe de Physique des Matériaux, Normandie Univ, UNIROUEN, INSA Rouen, CNRS, Avenue de l'Université, 76801 Saint Etienne du Rouvray Cedex, France
Université de Toulouse, Institut Clément Ader, ISAE-SUPAERO – UPS – IMT Mines Albi – INSA - 10 av. E. Belin, 31055 Toulouse cedex 4, France

Keywords:
Thermoplastic
Fracture toughness
Damage mechanics
Temperature
Mixed-mode

A B S T R A C T

The present work was aimed at investigating the failure of quasi-isotropic fibers reinforced thermoplastic laminates solicited at different testing temperatures. Single-edge-notch bending (SENB) tests were conducted at room temperature (RT) and at a temperature higher than the glass transition temperature (T_g) to investigate the influence of failure mode (depending on initial notch orientation) as well as matrix ductility and toughness (depending on testing temperature) on: (1) damage mechanisms – (2) critical translaminar fracture toughness G_c and (3) G-R curves evolution. The mixed mode fracture toughness $G_{I+II,c}$ is dramatically lower than the mode I fracture toughness G_{Ic}, with −52% and −67% decreases, at RT and 150 °C respectively. In 45° notched specimens, most of the fracture energy (about 80%) stems from the mode I failure. Though they are not prominent on fracture, the failure mechanisms associated with mode II are instrumental in limiting the contribution of mode I on fracture behavior. Finally, though a temperature increase has very little influence on G_{Ic}, it significantly reduces the value of $G_{I+II,c}$ (−32%). This change primarily results from the formation of plastic-kink bands in compression that are promoted by both the ductility of the polyether ether ketone (PEEK) matrix at $T > T_g$ and the mixed-mode failure.

1. Introduction

Edge cracks can initiate from notches at the surface of composite laminates due to processing (consolidation, machining) or stress concentrations due to the geometry of composite structures [1]. They may result in the failure of composite structures subjected to service conditions (monotonic or cyclic loadings). It is therefore necessary to evaluate the influence of prominent factors (notch orientation, stacking sequence, matrix ductility, service temperature) on the overstress distribution at the notch tip in order to better understand the subsequent damage mechanisms and failure modes (opening or mixed-mode). In orthotropic or quasi-isotropic composite laminates, transverse matrix cracking and fibers breakage (also known as translaminar failure modes) are usually the primary damage mechanisms occurring in the early phase of mechanical loading. A comprehensive review of techniques for the experimental characterization of the fracture toughness associated with the translaminar failure modes of continuously reinforced laminated composites is presented in [2]. Depending on matrix ductility, the localized matrix plasticization is an energy dissipative process ruling both fracture behavior and composite toughness, as these matrix-rich regions may act as cracks barriers and subsequent propagation in laminated fiber-reinforced plastics [3]. It is therefore expected this mechanism to reflect on material toughness measurements either in fiber-dominated laminates (quasi-isotropic) or matrix-dominated laminates (angle-ply).

1.1. Influence of temperature on fracture behavior

In the literature, the modes of energy dissipation are mainly affected by the matrix fracture mode (brittle or ductile) which is mainly determined by the loading rate or temperature conditions [4–5]. The energy dissipated during controlled crack propagation in carbon fibers reinforced composites is usually evaluated in terms of different source mechanisms: plastic deformation, fibre-snapping, matrix-cracking and fibre pull-out [6–7]. As far the crack initiation and propagation are concerned, it is therefore potentially interesting to associate fibers with highly ductile TP matrices [8], the effect of which is even more noticeable when service temperature is higher than the polymer glass

* Corresponding author at: Groupe de Physique des Matériaux, Normandie Univ, UNIROUEN, INSA Rouen, CNRS, Avenue de l'Université, 76801 Saint Etienne du Rouvray Cedex, France.
E-mail address: benoit.vieille@insa-rouen.fr (B. Vieille).

https://doi.org/10.1016/j.tafmec.2022.103414

transition temperature, even in QI laminates whose behavior is fiber-dominated [9]. Most references dealing with the translaminar fracture behavior concern thermosetting-based composites and the influence of temperature on the interlaminar fracture toughness has been widely addressed [10]. Munro et al have shown that the translaminar fracture energy of C/epoxy composites significantly increased with temperature (from 124 to 200 kJ/m^2, at room temperature and 80 °C respectively). Carbon-fiber pull-out energy represents 25% of the total fracture energy [5]. Garg has investigated the translaminar fracture behavior of graphite/epoxy laminates by conducting compact tension specimens on laminates with different lay-ups ($(90)_{16}$, $(0/90)_{4s}$, $(\pm45)_{4s}$, $(0/\pm45/90)_{2s}$). In $(\pm45)_{4s}$ and $(0/90)_{4s}$ laminates, fracture toughness decreases around room temperature, and around −23 °C in $(90)_{16}$ laminates [11]. In quasi-isotropic laminates, fracture toughness follows the trend of other laminates up to about 120 °C. Beyond this temperature, fracture toughness begins to increase. A similar fracture behaviour was observed in glass/epoxy laminated composites, with a particular attention paid to the effects of temperature and deformation rate on the strain energy release rate in mode I and mode I/II [12]. On carbon fiber reinforced vinylester composites, Jia et al have conducted static and dynamic three-point bending tests for testing temperatures ranging from −100 to 120 °C [13]. They concluded that the studied laminates are characterized by enhanced flexural strength, maximum deflection, and energy absorption at lower temperatures (−60 °C, −100 °C) while they show relatively poor performance at a higher temperature (100 °C). This behavior is attributed to the "brittle" nature of the polymer matrix at lower temperatures resulting in higher Young's modulus and smaller ultimate tensile strain.

Only a few references have specifically addressed the fracture behaviour of thermoplastic (TP) based composites. Considering hybrid carbon and glass fiber woven-ply reinforced polyether ether ketone quasi-isotropic laminates, Vieille et al have investigated the influence of temperature and constraint effect on the fracture mechanisms and toughness [14]. As failure is primarily driven by fibers breakage in tension and in tension/compression, it turns out that a temperature increase has very little influence on the mode I critical translaminar fracture toughness K_{Ic} though the ductility of polyether ether ketone matrix is exacerbated at T > Tg. It also appears that the constraint effect has very little influence on K_{Ic} as single-edge-notch tensile test and single-edge-notch bending specimens have virtually the same value (about 45 MPa.$\sqrt{m}$). From the evolution of the G-R curves at high temperature, the highly ductile behavior of the polyether ether ketone matrix at T > Tg provides a good intrinsic toughness to the material, and the bridging of translaminar crack by the glass fibers at the outer surfaces of laminates contribute to a moderate increase in its extrinsic toughness.

Depending on the laminates' stacking sequence of carbon reinforced thermoplastic (PPS) composites, a temperature increase (RT and 120 °C) results in doubling the translaminar fracture toughness in both quasi-isotropic (QI) and $[+/-45°]_7$ laminates. It is assumed that local PPS matrix enhanced plastic deformation at T > T_g is a prominent dissipative process that efficiently contributes to increase the fracture toughness of C/PPS composites [15].

1.2. Effect of notch orientation

The question of mixed mode fracture has already been specifically addressed in the literature, though most references focus on the analytical formulation of stress intensity factors for an inclined edge crack in orthotropic materials subjected to point forces. Based on weight functions and boundary element method, the mixed-mode stress intensity factor is computed in two-dimensional cracked bodies [16–25]. Most references available in the literature deal with tensile or bending specimens with 0° oriented initial notches [26–27] or 45° oriented notch [12,15,28–29]. The earliest study was proposed in the mid-seventies by Spencer et al to investigate the effect of notch and fibre orientation on the crack propagation in FRPs [30]. In woven-ply glass/epoxy laminates, Kaya et al have shown that the values of fracture toughness obtained in Mode I are respectively 78 % and 211 % higher than in mixed mode (Mode I/II), at the same temperature and deformation rate [12]. To investigate the influence of laminates' stacking sequence, Vieille et al have conducted tensile tests on 5-harness satin weave carbon fabric reinforced PolyPhenylene Sulphide (PPS) laminated composites with an initial edge notch in quasi-isotropic and angle-ply laminates [15]. Depending on the initial notch orientation (0 or 45°), the total strain energy release rate in quasi-isotropic laminates is 6 times as low as in $[+/-45°]_7$ laminates, suggesting that large plastic deformation (due to a matrix-driven behavior and an exacerbated matrix ductility at T > T_g) are instrumental in dissipating a great portion of the mechanical energy brought to the specimen.

1.3. Fracture toughness in anisotropic materials: Theoretical background

Depending on the matrix nature and the laminates' stacking sequence, the fracture mechanics analysis usually depends on the type of the fracture response (brittle or ductile) observed in composite laminates [31]. In elastic brittle composite materials, fracture is usually analyzed by using the Linear Elastic Fracture Mechanics (LEFM) parameters: *R*-curve analysis, critical strain energy release rate G_{Ic}, stress intensity factor K_{Ic}. The use of LEFM to describe damage as the propagation of a single dominant crack may be not always self-similar in heterogeneous composite materials depending on its stacking sequence [1]. In quasi-isotropic laminates with an elastic-brittle behavior, the translaminar crack growth resulting from an initial edge-notch is usually self-similar [14].

1.3.1. Fracture analysis in mixed-mode

Different approximations were proposed in the literature for measuring the mode I stress intensity factor K_I, which is classically estimated by analytical functions for single-edge-notched specimens [32]:

$$K_I = \sigma\sqrt{\pi a}\cdot F(a/w) \tag{1}$$

where σ is the remote applied stress, a denotes the length of the initial crack and w is the specimen width. $F(a/w)$ is a geometric finite-width-correction (FWC) function calculated from the ratio a/w and empirical formulas [14]. By definition, this FWC function is a scale factor applied to multiply the notched infinite-plate solution to obtain the notched finite-plate result [33]. In the case of bending specimens with an oblique initial notch, the following expressions have been proposed by Fett et al from approximate weight functions to account for mixed-mode (I + II) fracture [29]:

$$K_I = \sigma F_{I,b}\sqrt{\pi a} \quad \text{and} \quad K_{II} = \sigma F_{II,b}\sqrt{\pi a} \tag{2}$$

where the analytical geometric functions $F_{I,b}(a/w)$ and $F_{II,b}(a/w)$ can be obtained from weight functions in tension as functions of the notch orientation θ:

$$F_{I,b} = F_{I,t}\left[1 - \frac{4}{5}(a/w)\cdot cos\theta\right] - \frac{16}{15}\frac{\sqrt{2}}{\pi}(a/w)cos^3\theta$$

$$F_{II,b} = F_{II,t}\left[1 - \frac{4}{5}(a/w)\cdot cos\theta\right] - \frac{16}{15}\frac{\sqrt{2}}{\pi}(a/w)cos^2\theta sin\theta$$

where

$$F_{I,t}(a/w) = \frac{\sqrt{2}}{\pi}\left[2 + \frac{2}{3}A\left(\frac{a}{w}\right)\right]cos^2\theta \quad \text{and} \quad F_{II,t}(a/w) = \frac{\sqrt{2}}{\pi}\left[2 + \frac{2}{3}B(a/w)\right]cos\theta sin\theta$$

In which the functions $A(a/w)$ and $B(a/w)$ are defined by:

$$A(a/w) = 0.3515 + 0.2851(a/w) - 0.1723(a/w)^2 + 1.212(a/w)^3$$

$$B(a/w) = 0.04362 - 0.0883(a/w) - 0.8302(a/w)^2 + 0.19617(a/w)^3$$

1.3.2. Evaluation of fracture toughness in mixed-mode

In elastic brittle materials, it is possible to estimate the fracture toughness in mode I from Single-Edge Notched (SEN) specimens [32–34]. Sih et al proposed a method to determine the stress-intensity factors K_i which can be related to the energy release rates G_i ($i = 1, 2, 3$). The relationships between K_i and G_i form the basis of the equivalence of the Griffith energy theory and the current stress intensity factor approach in fracture mechanics. If the material is orthotropic with the crack on one plane of symmetry, the three basic modes are conveniently independent. In the case of plane stress conditions, if the first two modes are present together then:

$$G_{tot} = G_I + G_{II} \tag{3}$$

where the strain energy release rates in mode I and II are defined from the engineering constants by:

$$G_I = C_I \cdot K_I^2 \quad \text{and} \quad G_{II} = C_{II} \cdot K_{II}^2 \tag{4}$$

$$\text{With } C_I = \sqrt{\frac{1}{2E_xE_y}}\sqrt{\sqrt{\frac{E_x}{E_y}} - \nu_{xy} + \frac{E_x}{2G_{xy}}} \text{ and } C_{II} = \frac{1}{E_x\sqrt{2}}\sqrt{\sqrt{\frac{E_x}{E_y}} - \nu_{xy} + \frac{E_x}{2G_{xy}}}$$

where E_x, E_y, G_{xy} and ν_{xy} are the in-plane mechanical properties of the equivalent orthotropic material [32].

Finally, the critical fracture toughness in mode I G_{Ic} or mixed-mode $G_{I+II,c}$ corresponds to the values of the strain energy release rate at crack initiation.

1.3.3. Evaluation of the G-R curves

To characterize the fracture behavior of materials, the knowledge of the so-called G-R curves if utmost important for design purposes as it represents the evolution of the strain energy release rate along with the macroscopic crack length. The computation of the fracture energy primarily and corresponding data reduction methods depend on the fracture nature (brittle or ductile) as was detailed in [2]. In the present work, the SENB specimens with a quasi-isotropic lay-up are characterized by a gradual failure. Thus, the G-R curves were computed from the compliance loss C(corresponding to the displacement over load ratio at any time of the mechanical testing) and the corresponding gradual crack growth in agreement with the ASTM standard test method E1820 [35]. In order to calculate the strain energy release rate, the compliance method was applied [36–39]. In accordance with the ASTM standard test method, the use of LEFM requires a linear load–displacement behavior and very localized plastic deformation at the crack tip [35]. The later condition seems to be satisfied in quasi-isotropic laminates considering the macroscopic mechanical response of SENB specimens. The relationship between the compliance and the crack length a is classically associated with the calculation of the strain energy release rate G by the following expression:

$$G = \frac{P^2}{2b}\frac{dC}{da} \tag{5}$$

In Eq. (5), b is the thickness of the laminate and P is the applied force. From Eq. (5), it is therefore possible to compute the strain energy release rate in mode I and mixed-mode. The crack growth is evaluated by means of a digital images' analysis detailed in Section 2.2.2.

Table 1
A few properties of woven carbon and glass fibers reinforced PEEK elementary ply at RT [14].

	Carbon/PEEK	Glass/PEEK
E_x(GPa)	60	22
E_y(GPa)	60	20
G_{xy}(GPa)	4.8	6.55
ν_{xy}	0.04	0.04
Tensile strength (warp) (MPa)	963	1172
Compressive strength (warp) (MPa)	725	1103
Nominal ply thickness (mm)	0.31	0.25
Tg (°C)	145	145

Table 2
Mechanical properties of the equivalent orthotropic material – Quasi-isotropic CG/PEEK laminates.

	E_x(GPa)	E_y(GPa)	G_{xy}(GPa)	ν_{xy}	C_I(GPa^{-1})	C_{II}(GPa^{-1})
RT	39.45	39.45	18.24	0.35	0.0236	0.0254
150 °C	36.58	36.58	16.92	0.35	0.0236	0.0254

1.4. Objectives of the study

This work is aimed at investigating the fracture behavior of hybrid fibers reinforced laminated composites consisting of highly ductile thermoplastic matrix (PEEK) and brittle fibers (carbon and glass woven fabrics). The effect of temperature and fracture mode on the fracture toughness and crack growth of the laminates are specifically addressed. On the one hand, bending tests were carried out at room temperature (RT) and at 150 °C (i.e. slightly higher than T_g as the ductile behavior of PEEK matrix is exacerbated) to examine the influence of temperature on PEEK matrix toughness and ductility; therefore, on fracture energy. On the other hand, SENB specimens with two different initial notch orientations (0° and 45° oriented notches) to evaluate the mixed-mode fracture toughness as well as crack propagation. Finally, the G-R curves were computed from the compliance method to investigate the influence of failure mode on energy dissipative processes and corresponding fracture toughness.

2. Materials and experimental set-up

2.1. Materials and specimens

The consolidated laminates consist of 14 inner carbon-PEEK plies and two outer glass-PEEK plies provided by Toho Tenax [14]. The two-outer glass-PEEK plies are considered for electrical protection purposes. The carbon and glass fiber woven fabrics are balanced in the warp and weft directions. The PolyEther Ether Ketone (PEEK) matrix has a glass transition temperature $T_g = 143$ °C. The laminated plates obtained by thermo-compression are made up of carbon–PEEK 5HS woven plies prepregs and glass–PEEK prepregs. The stacking sequence of laminates is quasi-isotropic: $[(0/90)_G,[(0/90),(\pm45)]_3,(0/90)]s$ (with G index for glass fibers ply). The mechanical properties of C/PEEK and G/PEEK elementary plies are specified in Table 1.

The in-plane mechanical properties of the equivalent orthotropic material at RT and 150 °C, required to compute the coefficient C_I (Eq. (4)), are given in Table 2.

The bending test specimens were cut by water jet from 600 × 600 mm^2 plates. The average width and thickness (calculated from five measurements each) is virtually constant for all specimens: 15 ± 0.05 mm and 4.5 ± 0.06 mm, respectively. SENB specimens are characterized by two different orientations of the initial notch (Fig. 1) in order to observe a purely mode I failure (0° oriented notch) or a mixed mode failure (45° oriented notch). The 0° SENB specimens are characterized by a ratio $a/w = 0.33$, whereas the 45° SENB specimens have a ratio $a/$

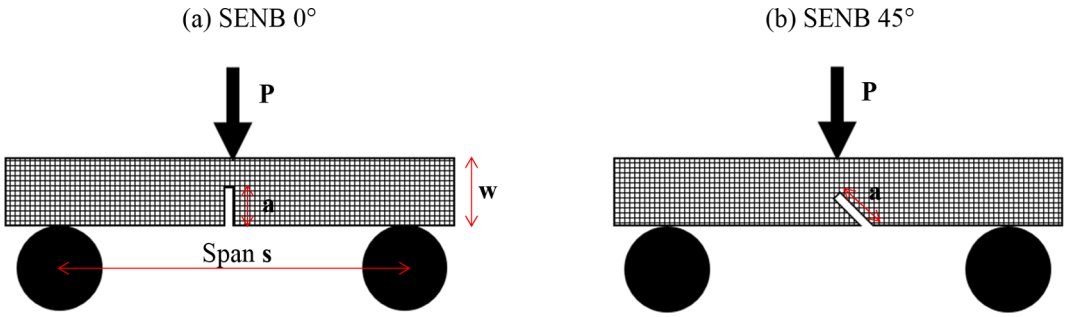

Fig. 1. Single-Edge Notched bending specimens: (a) 0° initial notch – (b) 45° initial notch.

Fig. 2. Experimental set-up showing the DIC technique at high temperature.

$w = 0.48$ so that the projected area is the same. Notches were machined by means of a precision endless diamond wire saw whose radius is 0.085 mm. Three specimens were tested in each configuration. The average specimen's thickness (4.5 mm) is significant enough to consider the sample as thick structures in which a plane strain state prevails.

2.2. Method and experimental set-up

2.2.1. Mechanical testing

SENB specimens were subjected to monotonic bending loadings at room temperature and at 150 °C, by means of a MTS 810 servo-hydraulic testing machine equipped with a 100kN capacity load cell and a thermal chamber. The bending tests were conducted in displacement-controlled mode with a loading rate of 2 mm/min (quasi-static loading conditions). The mechanical properties in bending were determined according to the European standards EN 2562 [40]. The bending strain and stress are defined as follows:

$$\varepsilon_{bending} = \frac{6dw}{s^2} \quad \text{and} \quad \sigma_{bending} = \frac{3Fs}{2bw^2} \tag{6}$$

where b is specimen thickness, w is the specimen width, s is the span between the support points (80 mm), F is the load measured by the load cell during the bending test and d is the displacement applied to the lower part of the specimen (Fig. 1).

2.2.2. Full-field measurements

A two-dimensional Digital Image Correlation (DIC) technique is used to measure full-field strains. A high-speed monochromic camera Phantom Miro M310 records digital images during thermomechanical loading. The acquisition frequency is 3,200 frames-per-second at full resolution (1280 × 800 pixels). The Green-Lagrange strain field is computed from the 2D displacement field by means of the VIC-2D correlation software (provided by the company Correlated Solutions). The use of DIC at high temperature requires a high intensity source combined with a fiber optic light guide directly placed into the thermal chamber (Fig. 2). The DIC technique compares the digital images for various small regions (known as subsets) throughout the images before and after deformation using fundamental continuum mechanics concepts, locating the positions of each of these subsets after deformation through digital image analysis. When a material discontinuity appears in the pattern, the homogeneous linear mapping in this region does not present deformed surface and the small subset position is not computed. Using an algorithm implemented in the Scilab code, the crack tip is located via the discontinuity of the strain field resulting from the crack propagation (Catalanotti et al. used a similar technique based on the displacement discontinuity within the pattern [41]). Scilab is a free and open-source, cross-platform numerical computational package and a high-level, numerically oriented programming language [42].

A binarization of the full-field strain obtained by the VIC-2D software is applied. The identification of the damaged and undamaged areas in the region of interest is associated with a F_T function defined by:

$$\forall \boldsymbol{\varepsilon}_{xy}(\boldsymbol{x},\boldsymbol{y}) \neq 0 \Rightarrow \mathbf{F_T}(\boldsymbol{x},\boldsymbol{y}) = 0$$

$$\forall \boldsymbol{\varepsilon}_{xy}(\boldsymbol{x},\boldsymbol{y}) = 0 \Rightarrow \mathbf{F_T}(\boldsymbol{x},\boldsymbol{y}) = 1 \text{ or } \mathbf{F_T}(\boldsymbol{x},\boldsymbol{y}) = -1$$

One may specify that: $\boldsymbol{F_T} = 0$ corresponds to the region for the undamaged area. $\boldsymbol{F_T} = 1$ is the damaged area where a material discontinuity is present near the initial crack tip. $\boldsymbol{F_T} = -1$ is the damaged area where material discontinuity appears due to a secondary crack. The crack length is then determined from the crack tip position in each pattern, independently of the orientation of crack within the pattern. The spatial resolution of the crack length is defined by the size of the

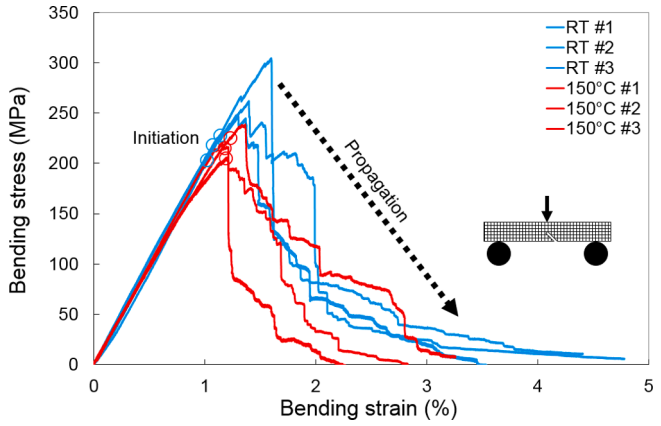

Fig. 3. Influence of temperature on the tensile response and the fracture behaviour (initiation and propagation) of SENB specimens with a 45° initial notch.

Table 3
Influence of temperature on the ultimate bending strength and the bending strain at crack initiation.

	Mode I	Mixed-mode (I + II)		
	$\sigma^{u}_{bending}$(MPa)	$\sigma^{u}_{bending}$(MPa)	$\sigma^{initiation}_{bending}$(MPa)	$\varepsilon^{initiation}_{bending}$(%)
RT	305 ± 16	271 ± 29	216 ± 12	1.08 ± 0.06
150 °C	290 ± 14	196 ± 27	215 ± 10	1.20 ± 0.03

subsets used in the DIC method.

2.2.3. Fractographic analyses

Fracture mechanisms are discussed by means of fractographic analyses based on microscopic observations done with a Keyence optical microscope.

3. Results and discussion

3.1. Influence of testing temperature on fracture behavior

The macroscopic bending response of notched quasi-isotropic laminates is virtually elastic up to the ultimate strength. The load borne by the specimen significantly drops then and a quasi-brittle fracture behavior is observed along with a gradual decrease in the load as the macroscopic crack propagates (Fig. 3).

The ultimate value $\sigma^{u}_{bending}$ is computed from the peak value on the curves shown in Fig. 3, and the initiation value $\sigma^{initiation}_{bending}$ is computed from the value of the force corresponding to the initiation point (Table 3). From the macroscopic mechanical properties' standpoint, it appears that the ultimate bending strength significantly decreases (about −20% - Table 3) as testing temperature increases. However, the stress at crack initiation is unchanged, whereas the strain at initiation slightly increases (about +10%). It is worth noting that crack initiation is approximately determined near the initial notch tip from the real-time observation of the specimen's surface by means of the CCD camera (see Section 2.2.2). As the tests were conducted in displacement-controlled mode, the change in bending strain at initiation suggests that temperature contributes to delay the onset of damage. The ultimate strength being reached for strain values higher than the ones at initiation, it indicates that the damage resulting from crack initiation is subcritical as the specimen is still able to bear a mechanical load at macroscopic level. Therefore, we may wonder what are the underlying mechanisms ruling the crack propagation until the macroscopic load starts gradually decreasing (critical damage). Thus, the crack propagation consists of two different stages: a first one associated with subcritical damage and a second one associated with critical damage mechanisms. This question will be specifically addressed in Section 3.3.

Table 4
Influence of temperature on the critical fracture toughness of hybrid CG/PEEK laminates in bending:(a) mode I (0° notch) – (b) mixed mode (45° notch).

	(a) Mode I	(b) Mixed mode			
	G_{Ic}(kJ/m²)	G_I (kJ/m²)	G_{II}(kJ/m²)	$G_{I+II,c}$(kJ/m²)	Influence of failure mode
RT	52.92 ± 4.99	20.94 ± 6.63	4.32 ± 1.54	25.26 ± 8.17	−52%
150 °C	52.07 ± 3.16	14.18 ± 5.44	2.91 ± 1.21	17.09 ± 6.65	−67%
Influence of T°	~			−32%	

The influence of temperature on the fracture behavior of SENB specimens with a 0° initial notch was discussed in a previous work [14]. It was concluded that mode I failure is primarily driven by the breakage of 0°oriented fibers in tension/compression. As a result, a temperature increase (from RT to 150 °C – same testing temperature conditions as the ones considered in the present work) has very little influence on the mode I critical fracture toughness G_{Ic} though the ductility of the PEEK matrix is exacerbated at T > Tg. The fracture toughness values in mode I and mixed mode (I + II) are computed from Eqs. (1)–(4). From the values shown in Table 4, it appears that the mode I critical strain energy release rate is virtually unchanged (+7%), whereas the equivalent fracture toughness in mixed mode dramatically decreases (−32%) as testing temperature increases. The reasons for this dramatic change will be further investigated by the examination of the damage mechanisms taking place within SENB specimens having 45° oriented initial notches. In particular, it is assumed that PEEK matrix ductility may promote energy dissipative processes via local plastic deformation mechanisms.

3.2. Influence of failure mode (notch orientation) on fracture behavior

As far the translaminar fracture behaviour of laminated composites is concerned, there is no specific recommendation on the pre-cracking of specimens in test standards. In the present work, the purpose of the singularity is only to create a stress concentration near the original notch tip where the crack will be initiated. Indeed, the theoretical background described in Section 1 refers to the initiation of a crack from a stress concentrator. Of course, the local stress state will significantly depend on the initial notch tip radius, the Eqs. (1)–(5) do not explicitly consider this parameter. It is worth noting that the induced damage mechanisms could completely change in the presence of an actual crack. One may recall the initial notch orientation (0 or 45° oriented notch) machined in quasi-isotropic SENB specimens is expected to induce purely mode I and mixed-mode (I + II) failures, respectively. From the macroscopic behavior standpoint (Fig. 4), the notch orientation seems to have little influence on the stress–strain response, as the mechanical behavior is elastic up to ultimate load, which is lower in mixed-mode (about −15% at RT and −30% at 150 °C – see Table 3). A very gradual drop of the load borne by the specimens then follows it. As was mentioned in the previous section, the damage mechanisms resulting from a mixed-mode failure are sensitive to testing temperature.

The stress intensity factor values being computed from ultimate strength values (Eqs. (1)–(2)); these strengths are expected to reflect on the critical fracture toughness values (Eqs. (3)–(4)) as well as the temperature-dependence of the elastic constants (Table 2). Thus, the ultimate strength is about 10% and 30% lower in 45° notches specimens with respect to 0° notched specimens, at RT and 150 °C respectively (Table 3). The comparison of mode I and mixed-mode failures values shows that the critical strain energy release rate significantly decreases (-52%) at RT. The change is even more dramatic at 150 °C with a −67% decrease (Table 4). Ultimately, these results clearly indicate that the

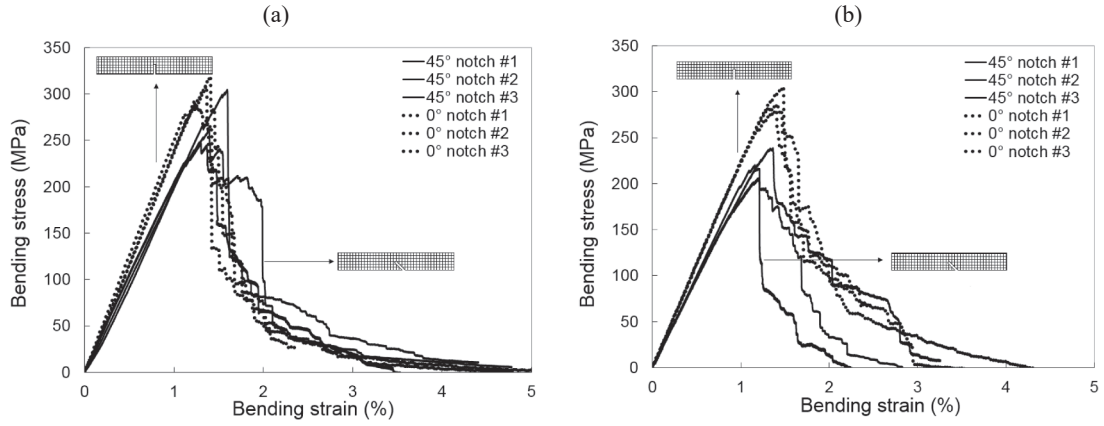

Fig. 4. Influence of initial notch orientation on the tensile response and the fracture behavior of SENB specimens: (a) RT – (b) 150 °C.

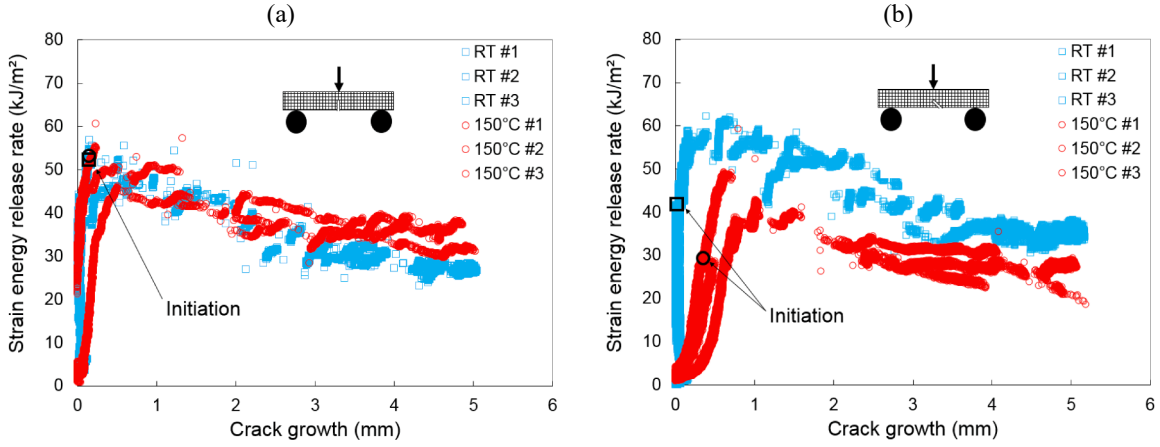

Fig. 5. Influence of failure mode (notch orientation) on the fracture behavior represented by the G-R curves in SENB specimens: (a) RT – (b) 150 °C.

fracture toughness in mode I, which is an opening failure mode, is a lot higher than the fracture toughness in mixed-mode. Under the same loading conditions, it indicates that the capability of damage mechanisms to dissipate the mechanical energy brought to the specimen are different depending on the failure mode. In SENB specimens with a 45° initial notch, it is also important noting that modes I and II represent about 82% and 18% of the fracture energy, respectively. This suggests that mode I prevails in the fracture behavior of these specimens, and it is expected to reflect on the failure surface. The corresponding fracture toughness in mode I is approximately half the value of the one estimated

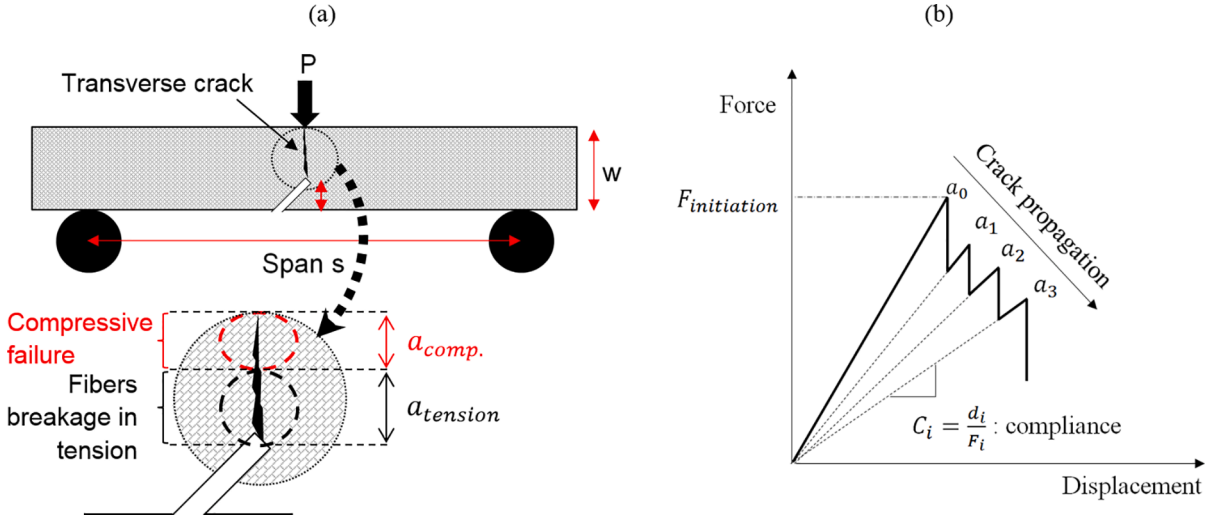

Fig. 6. Crack propagation in tension and in compression within SENB specimens with a 45° initial notch: (a) Illustration of the fracture process zone (FPZ) in bending – (b) Compliance loss coming along with gradual crack propagation.

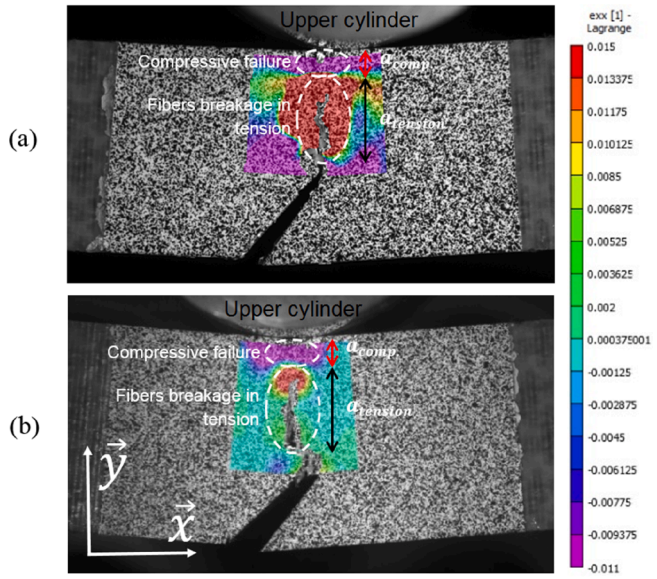

Fig. 7. Influence of testing temperature on the Green Lagrange longitudinal strain field in SENB specimens with a 45° initial notch: (a) RT – (b) 150 °C. (For interpretation of the references to colour in this figure legend, the reader is referred to the web version of this article.)

in purely mode I failure (Table 4).

Finally, the G-R curves were computed from the compliance method (Eq. (5)) introduced in Section 1.3.3. At both testing temperatures, the G-R curves evolutions are similar in terms of curves shape and values (G and crack growth) in mode I and mixed-mode: the strain energy release rate gradually decreases as crack length increases (Fig. 5). In 45° notched specimens, the crack growth is very sudden at RT, whereas it turns out to be very gradual at 150 °C. These evolutions are consistent with the gradual compliance loss observed on stress–strain curves. Indeed, the energy required for crack propagation (in tension and in compression) decreases as the crack grows, namely when the tensile and compressive cracks ultimately coalesce. With respect to the mixed-mode critical fracture toughness values (at initiation) obtained from the compliance method (Fig. 5), it appears that the values calculated with Eqs. (1)–(3) are about 30% lower (Table 4). The values calculated from the compliance method are based on macroscopic bending response in terms of force vs displacement. This approach makes no distinction between the mode I and mode II failure modes, whereas the analytical approach proposed by Fett separates the contribution of each failure to the fracture energy. This method does not consider the mutual interactions of failure modes. It is also assumed that the mode I value is probably underestimated as suggested by the transverse (mode I) cracking shown in Fig. 11. As was underlined in Sections 3.1 and 3.2, the fracture behavior is virtually temperature-independent in specimens experiencing mode I failure. The main reason is that mode I failure is primarily driven by the breakage of 0°oriented fibers in tension/

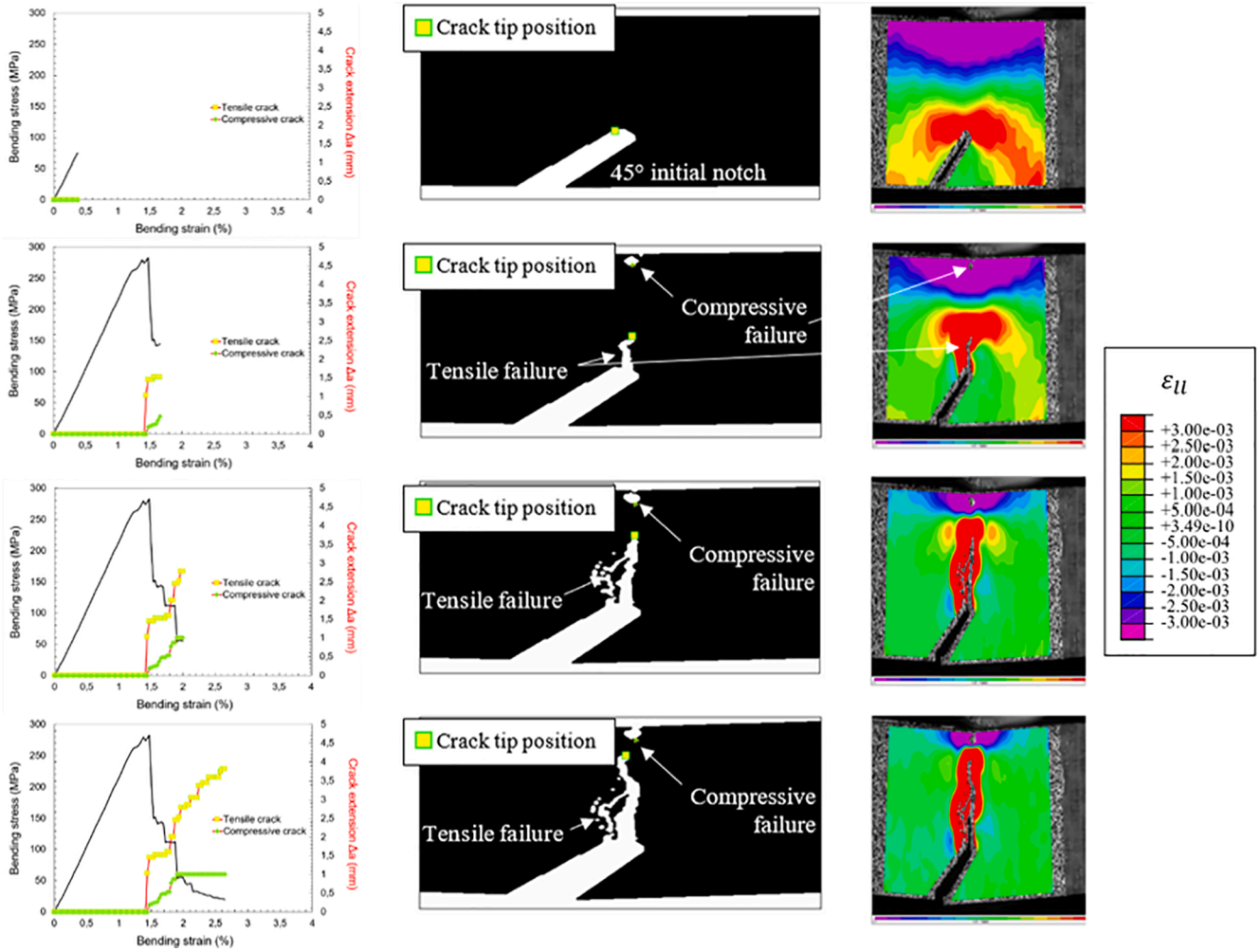

Fig. 8. Evaluation of the crack length from the crack tip position during loading: (a) stress–strain behavior along with crack growth – (b) Binarization of Digital Images – (c) Digital Image Correlation showing the axial strain distribution.

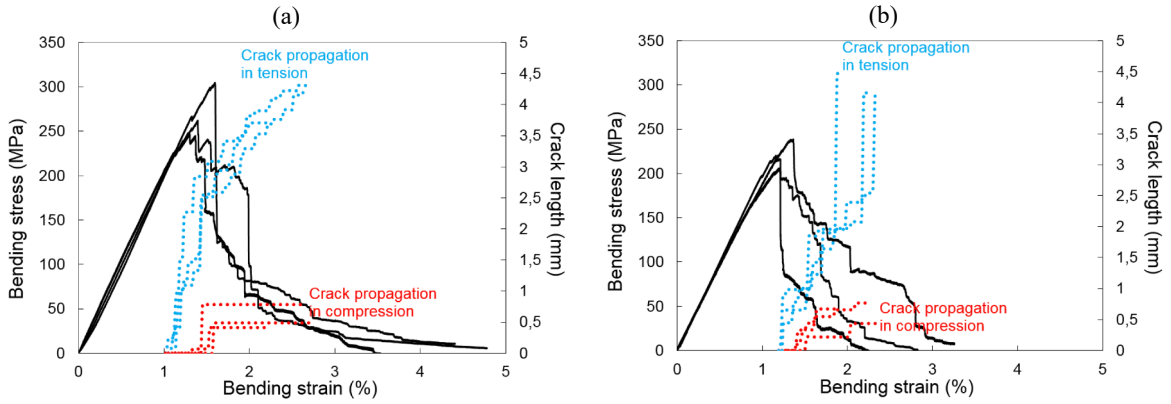

Fig. 9. Evolution of crack initiation and propagation in tension and in compression in SENB specimens with a 45° initial notch: (a) RT – (b) 150 °C.

Table 5
Mechanical properties in tension and compression of unnotched CG/PEEK quasi-isotropic laminates depending on testing temperature.

	Tension			*Compression*		
	$E_x(GPa)$	$\sigma_x^u(MPa)$	$\varepsilon_x^u(\%)$	$E_x(GPa)$	$\sigma_x^u(MPa)$	$\varepsilon_x^u(\%)$
RT	52.57 ± 0.58	784 ± 22	1.52 ± 0.04	49.25 ± 0.50	573 ± 13	1.75 ± 0.07
150 °C	48.30 ± 1.16	664 ± 29	1.33 ± 0.08	47.75 ± 1.20	434 ± 22	1.36 ± 0.04

compression. However, a major difference is observed in the influence of testing temperature on the fracture behavior in mixed-mode (Fig. 5b). The failure mechanisms in mixed-mode will be investigated in the next section, as well as their temperature-dependence.

3.3. Investigations on failure mechanisms in mixed-mode

More specifically, it appears that the gradual decrease (associated with compliance loss C_i) in the transverse load F_i applied to SENB specimens comes along with a stable transverse crack propagation (Fig. 6b). The transverse crack actually corresponds to simultaneous failure mechanisms: (1) a compressive failure in the upper part of the specimen (the one below the contact area between the upper cylinder allowing the application of the transverse force) and (2) a breakage of 0° fibers in tension near the crack tip (Fig. 6a and 7).

The Digital Image Correlation technique (described in Section 2.2.2) gives the distribution of the axial Green-Lagrange strain (Fig. 7) in the fracture process zone (FPZ). The dimensions of the FPZ corresponding to failure mechanisms in tension and in compression clearly appear in Fig. 7. An *in-situ* crack growth measurement and a binarization algorithm were used to determine the crack length from the crack tip position in each pattern.

From the binarization of the Digital Images (Fig. 8), the transverse cracks initiation and propagation in both tension (positive strains values) and compression (negative strains values) can be evaluated along with the load borne by the specimen (Fig. 9). The tension crack initiates earlier at RT whereas the compression crack initiation appears to be temperature-independent. The evolutions of cracks lengths in tension and in compression make it possible to compare the contribution of tensile and compressive failures on macroscopic fracture. For both testing temperature conditions, it appears that the crack initiates first in tension and tensile failure remains prominent during loading. Compressive cracks seem to initiate later when the transverse load

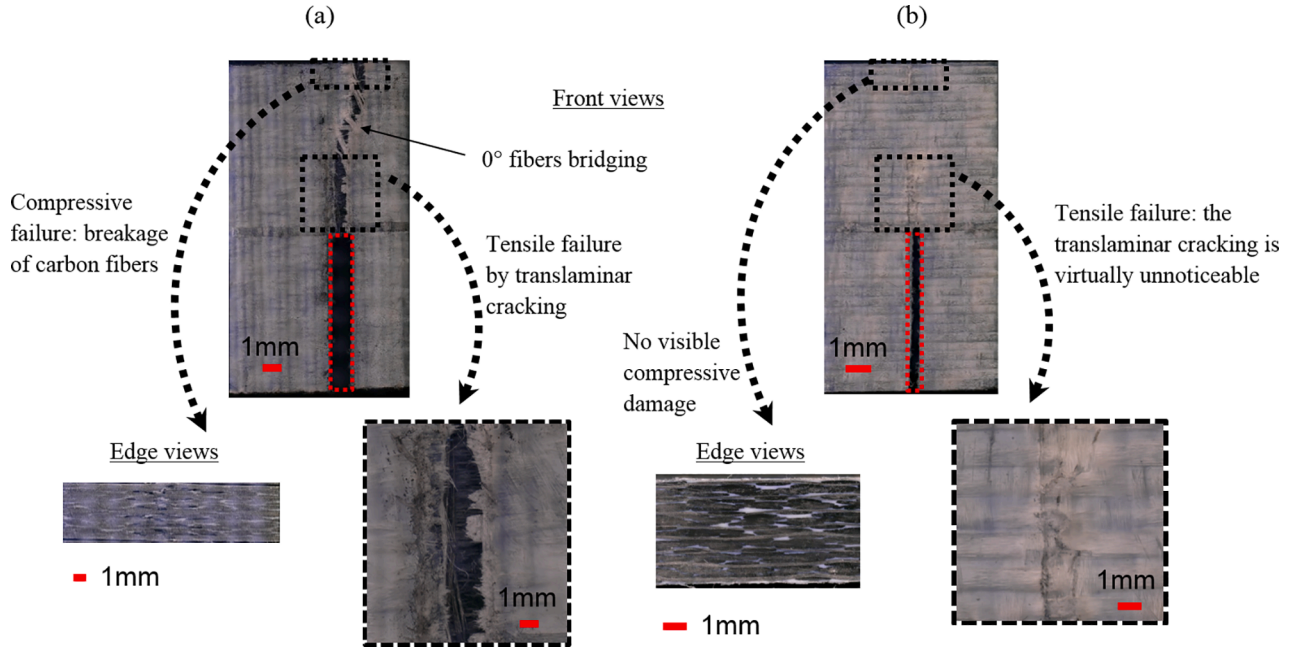

Fig. 10. Microscopic observations of fracture process zones in SENB specimens with a 0° initial notch: (a) RT – (b) 150 °C.

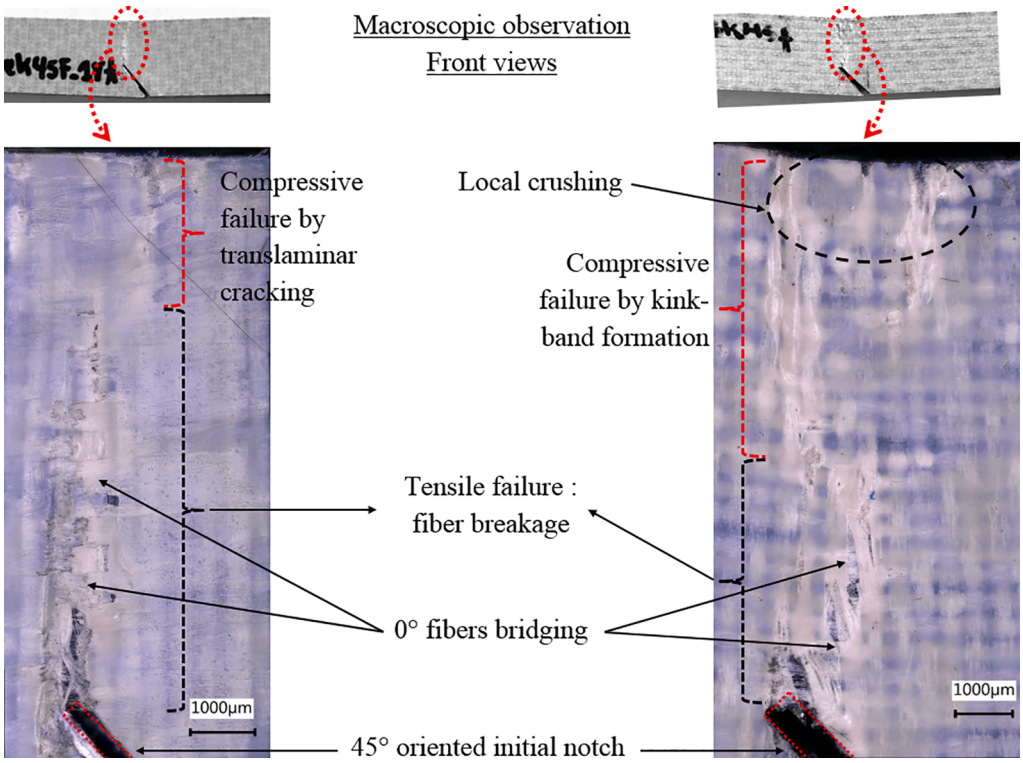

Fig. 11. Macroscopic and microscopic observations of the fracture process zones on the outer surface of SENB specimens with a 45° initial notch: (a) RT – (b) 150 °C.

reaches its ultimate value. Compared to compression the crack growth is different in tension depending on testing temperature. In tension, the crack growth is gradual at both temperatures and ultimately reaches about 4 mm (that is almost half of specimen width). Indeed, after initiation, the compressive crack immediately reaches a plateau (about 0.5 mm) at RT, whereas the crack growth is more gradual before reaching a plateau at about 0.5 mm. The reasons for this plateau will be further discussed along with the microscopic observations of fractured surfaces.

The influence of testing temperature on tensile and compressive failure mechanisms can be discussed considering the mechanical properties of unnotched laminates (Table 5). The ultimate tensile strength

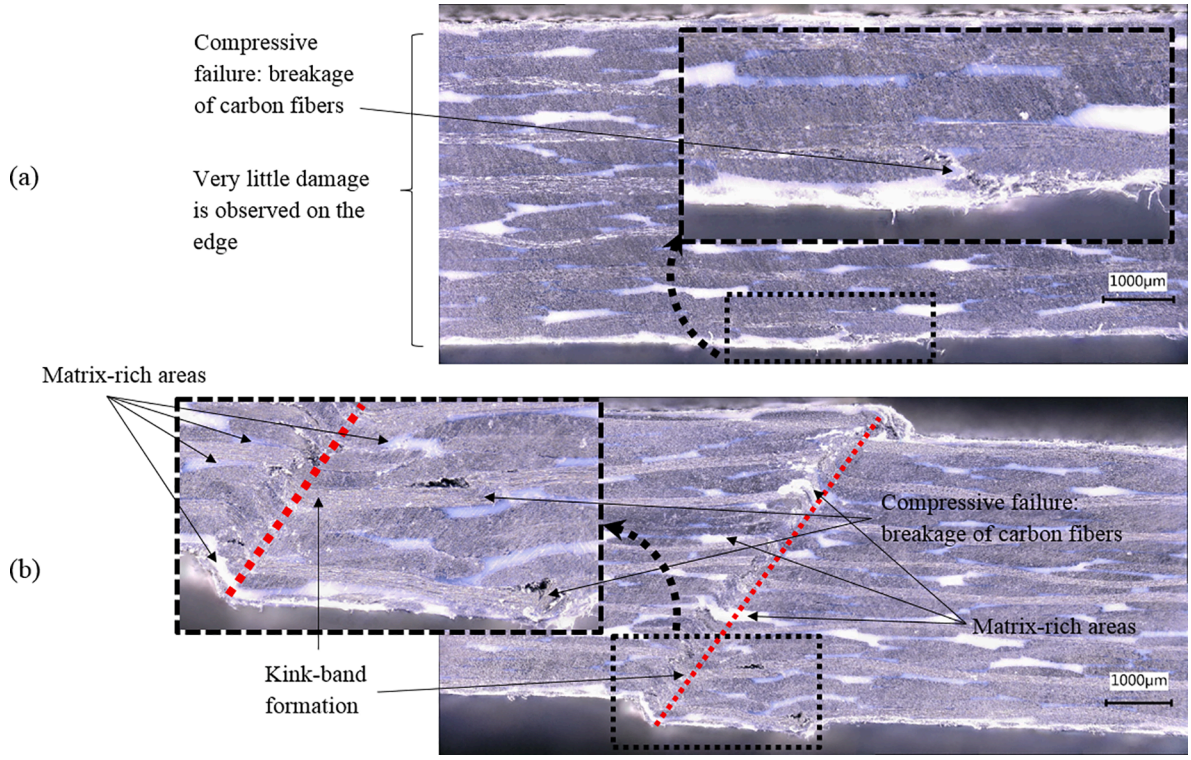

Fig. 12. Microscopic observations of the fracture process zones on the upper edge of SENB specimens with a 45° initial notch: (a) RT – (b) 150 °C.

decreases by 15% and 25%, at RT and 150 °C respectively. It therefore suggests that the local compressive failure induced by the upper cylinder allowing the application of the transverse force will be promoted by a temperature increase. The contribution of compressive failure to mixed-mode fracture is expected to be more important at 150 °C.

In order to understand the contribution of tensile and compressive failures to fracture mechanisms in mode I and mixed-mode, microscopic observations of fractured surfaces have been carried out. As was discussed in [14], the mode I failure is clearly driven by the breakage of 0°oriented fibers in tension/compression (Fig. 10). It therefore justifies why the mode I failure is temperature-independent.

In specimens experiencing a mixed-mode failure, most of the fracture energy (about 80%) stems from the mode I failure. This indicates that mode I prevails in the fracture behavior of these specimens, and it is expected to reflect on the failure surface. Indeed, the translaminar cracking appears to be transverse though the initial notch is oriented at 45° (Fig. 11).

It was assumed previously that mode I value is probably underestimated (Table 4) as suggested by the transverse (mode I) cracking shown in Fig. 11. In addition, the corresponding fracture toughness in mode I is approximately half the value of the one estimated in purely mode I failure (Table 4). Though they are not prominent on fracture, it therefore suggests that the failure mechanisms associated with mode II are instrumental in limiting the contribution of mode I on fracture behavior. In mixed-mode failure, as was pointed out by the DIC analysis, the transverse cracks propagate in both tension and compression (Fig. 11). The post mortem observations of failure surfaces suggest that compressive failure becomes prominent as temperature increases. At RT, there is virtually no damage in the contact area between the upper cylinder allowing the application of the transverse force and the specimen's edge (Fig. 12a). Only a moderate breakage of 0° carbon fibers is observed near the free surface of the laminates. At 150 °C, compressive failure results from the formation of a plastic kink-band that is clearly observed through the thickness of the laminate (Fig. 12b). Some breakage of 0° carbon fibers also comes along with the kink-bands formation.

As was underlined in Fig. 9b, just after initiation, the compressive crack immediately reaches a plateau at RT, suggesting that the primary damage mechanism ruling compressive failure corresponds to the formation of large plastic kink-bands. PEEK matrix ductility being enhanced at 150 °C, the formation of such plastic kink-band is more gradual at high temperature as matrix-rich areas undergo larger local plastic deformation. One may point out that PEEK matrix occasionally turns white during plastic deformation (Fig. 12b). At RT, it is assumed that PEEK matrix is not ductile enough to facilitate kink-band formation that comes along with local plastic deformation of polymer matrix within PMCs.

4. Conclusions

The opening question of this paper was to know if mixed-mode failure is associated with larger fracture energies with respect to mode I failure. In this aim, three points bending tests were conducted at room temperature (RT) and at a temperature higher than T_g on quasi-isotropic laminated specimens with 0 and 45° oriented initial notches.

The obtained results show that mode I failure is ruled by the breakage of 0° oriented fibers and is virtually temperature-independent. Mixed-mode failure significantly depends on testing temperature. Though a temperature increase has very little influence on G_{Ic}, it significantly reduces the value of $G_{I+II,c}$ (–32%). This change primarily results from the formation of plastic-kink bands in compression that are promoted by both the ductility of the polyether ether ketone (PEEK) matrix at $T > T_g$ and the mixed-mode failure. In addition, the mixed mode fracture toughness $G_{I+II,c}$ is dramatically lower than the mode I fracture toughness G_{Ic}, with −52% and −67% decreases, at RT and 150 °C respectively. In specimens experiencing a mixed-mode failure, most of the fracture energy (about 80%) stems from the mode I failure. Though they are not prominent on fracture, the failure mechanisms associated with mode II are instrumental in limiting the contribution of mode I on fracture behavior.

From the *in-situ* crack growth measurements, the tension crack initiates earlier at RT whereas the compression crack initiation appears to be temperature-independent. The evolutions of cracks lengths in tension and in compression make it possible to compare the contribution of tensile and compressive failures on macroscopic fracture. Just after initiation, the compressive crack immediately reaches a plateau at RT, suggesting that the primary damage mechanism ruling compressive failure corresponds to the formation of large plastic kink-bands. PEEK matrix ductility being enhanced at 150 °C, the formation of such plastic kink-band is more gradual at high temperature as matrix-rich areas undergo larger local plastic deformation.

CRediT authorship contribution statement

B. Vieille: Conceptualization, Methodology, Writing – original draft. **J.-D. Pujols-Gonzalez:** Conceptualization, Methodology, Writing – original draft. **C. Bouvet:** Conceptualization, Methodology, Writing – original draft.

Declaration of Competing Interest

The authors declare that they have no known competing financial interests or personal relationships that could have appeared to influence the work reported in this paper.

References

[1] K.L. Reifsnider, Damage and damage mechanics, in: K.L. Reifsnider (Ed.), Fatigue of Composite Materials, Elsevier Science Publishers B.V., 1990, 11–78.
[2] M.J. Laffan, S.T. Pinho, P. Robinson, A.J. McMillan, Translaminar fracture toughness testing of composites: a review, Polym. Test. 31 (3) (2012) 481–489.
[3] B. Vieille, W. Albouy, D. Bouscarrat, L. Taleb, High-temperature fatigue behavior of notched quasi-isotropic thermoplastic and thermoset laminates: influence of matrix ductility on damage mechanisms and stress distribution, Compos. Struct. 153 (2016) 311–320.
[4] B. Lauke, W. Pompe, Fracture toughness of short-fibre reinforced thermoplastics, Compos. Sci. Technol. 26 (1) (1986) 37–57.
[5] M. Munro, C.P.Z. Lai, The elevated-temperature dependence of fracture energy mechanisms by hybrid carbon-glass fiber reinforced composites, J. Mater. Sci. 26 (1988) 4701–4720.
[6] J.K. Wells, P.W.R. Beaumont, Crack-tip energy absorption processes in fibre composites, J. Mater. Sci. 20 (8) (1985) 2735–2749.
[7] J.K. Wells, P.W.R. Beaumont, The prediction of R-curves and notched tensile strength for composite laminates, J. Mater. Sci. 22 (4) (1987) 1457–1468.
[8] M. Kawai, M. Morishita, K. Fuzi, T. Sakurai, K. Kemmochi, Effects of matrix ductility and progressive damage on fatigue strengths of unnotched and notched carbon fiber plain woven roving fabric laminates, Compos. Part A 27 (1996) 493–502.
[9] S.J. Kim, J.Y. Cho, Role of matrix in viscoplastic behavior of thermoplastic composites at elevated temperature, AIAA Am. Inst. Aeronaut. Astronaut. J. 30 (10) (1992) 2571–2573.
[10] R. de Cássia Mendonça Sales, B.L. Rossi Dias Endo, M.V. Donadon, Influence of temperature on interlaminar fracture toughness of a carbon fiber-epoxy composite material, Adv. Mater. Res. 1135 (2016) 35–51.
[11] A.C. Garg, Effect of moisture and temperature on fracture behavior of graphite-epoxy laminates, Eng. Fract. Mech. 29 (2) (1988) 127–149.
[12] Z. Kaya, H.E. Balcıoğlu, H. Gün, The effects of temperature and deformation rate on fracture behavior of S-2 glass/epoxy laminated composites, Polym. Compos. 41 (11) (2020) 4799–4810.
[13] Z. Jia, T. Li, F.-P. Chiang, L. Wang, An experimental investigation of the temperature effect on the mechanics of carbon fiber reinforced polymer composites, Compos. Sci. Technol. 154 (2018) 53–63.
[14] B. Vieille, J.-D. Gonzalez, C. Bouvet, Fracture mechanics of hybrid composites with ductile matrix and brittle fibers: Influence of temperature and constraint effect, J. Compos. Mater. 53 (10) (2019) 1361–1376.
[15] B. Vieille, M. Chabchoub, C. Gautrelet, Influence of matrix ductility and toughness on strain energy release rate and failure behavior of woven-ply reinforced thermoplastic structures at high temperature, Compos. B Eng. 132 (2018) 125–140.
[16] F. Delale, I. Bakirtas, F. Erdogan, The Problem of an Inclined Crack in an Orthotopic Strip, Trans. ASME 46 (1979) 90–96.

[17] D.D. Raftopoulos, B. Farahmand, Determination of modes I and II stress intensity factors for oblique single edge cracks subjected to tension, Eng. Fract. Mech. 14 (4) (1981) 763–778.
[18] M.H. Aliabadi, D.P. Rooke, D.J. Cartwright, Mixed-mode Bueckner weight functions using boundary element analysis, Int. J. Fract. 34 (2) (1987) 131–147.
[19] E.E. Gdoutos, D.A. Zacharopoulos, E.I. Meletis, Mixed-mode crack growth in anisotropic media, Eng. Fract. Mech. 34 (2) (1989) 337–346.
[20] P.W. Tan, C.A. Bigelow, An improved boundary force method for analyzing cracked anisotropic materials, Eng. Fract. Mech. 34 (2) (1989) 341–357.
[21] C.W. Woo, Y.H. Wang, Analysis of an internal crack in a finite anisotropic plate, Int. J. Fract. 62 (3) (1993) 203–218.
[22] H.K. Kim, S.B. Lee, Stress intensity factors of an oblique edge crack subjected to normal and shear tractions, Theor. Appl. Fract. Mech. 25 (1996) 147–154.
[23] X. Yan, Stress intensives and propagation of mixed-mode cracks, Eng. Fail. Anal. 13 (6) (2006) 1022–1027.
[24] H.G. Beom, C.B. Cui, Oblique edge crack in an anisotropic material under antiplane shear, Eur. J. Mech. A. Solids 30 (6) (2011) 893–901.
[25] H.S. Jang, H.G. Beom, Oblique edge crack in an orthotropic material under thermal loading, Arch. Appl. Mech. 84 (12) (2014) 1903–1916.
[26] K. Chandra Shekar, B. Singaravel, S. Deva Prasad, N. Venkateshwarlu, B. Srikanth, Mode-I fracture toughness of glass/carbon fiber reinforced epoxy matrix polymer composite, Mater. Today:. Proc. 41 (2021) 833–837.
[27] S. Vantadori, A. Carpinteri, K. Głowacka, F. Greco, T. Osiecki, C. Ronchei, A. Zanichelli, Fracture toughness characterisation of a glass fibre reinforced plastic composite, Fatigue Fract. Eng. Mater. Struct. 44 (1) (2021) 3–13.
[28] S.E. Swartz, L.W. Lu, L.D. Tang, Mixed-mode fracture toughness testing of concrete beams in three-point bending, Mater. Struct. 21 (1) (1988) 33–40.
[29] T. Fett, Mixed-mode stress intensity factors for the oblique edge-crack in rectangular specimens, Int. J. Fract. 61 (1993) 3–10.
[30] B. Spencer, J.T. Barnby, The effects of notch and fibre angles on crack propagation in fibre-reinforced Polymers, J. Mater. Sci. 11 (1976) 83–88.
[31] B. Vieille, M. Chabchoub, D. Bouscarrat, C. Gautrelet, A fracture mechanics approach using Acoustic Emission technique to investigate damage evolution in woven-ply thermoplastic structures at temperatures higher than glass transition temperature, Compos. B Eng. 116 (2017) 340–351.
[32] H. Tada, P.C. Paris, G.R. Irwin, The Stress Analysis of Cracks Handbook, 3rd ed., ASME Press, January 2000.
[33] S.C. Tan, Stress Concentration in Laminated Composites, Technomic Pub. Co., Lancaster, Pa., 1994.
[34] G.C. Sih, P.C. Paris, G.R. Irwin, On cracks in rectilinearly anisotropic bodies, Int. J. Fracture Mech. 1 (3) (1965) 189–203.
[35] ASTM standard E1820 test method, Standard Test Method for Measurement of Fracture Toughness.
[36] J.G. Williams, Introduction to linear fracture mechanics, in: D.R. Moore, A. Pavan, J.G. Williams (Eds.), Fracture Mechanics Testing Methods for Polymers, Adhesives and Composites, Elsevier Sci. Ltd, Oxford, UK, 2001, pp. 27–58.
[37] A. Pavan, Determination of fracture toughness (GIc and KIc) at moderately high loadings rates, in: D.R. Moore, A. Pavan, J.G. Williams (Eds.), Fracture Mechanics Testing Methods for Polymers, Adhesives and Composites, Elsevier Sci. Ltd, Oxford, UK, 2001, pp. 27–58.
[38] J.T. Barnby, B. Spencer, Crack propagation and compliance calibration in fiber-reinforced polymers, J. Mater. Sci. 11 (1976) 78–82.
[39] D.A. Jablonski, B. Journet, R.S. Vecchio, R. Hertzberg, Compliance functions for various fracture mechanics specimens, Eng. Fract. Mech. 22 (5) (1985) 819–827.
[40] Test standard EN 2562, Aerospace series – Carbon Fiber reinforced plastics – Test Method – Unidirectional laminates, flexural test parallel to the fiber direction. Published by the European Association of Aerospace Industries (AECMA), March 1997.
[41] G. Catalanotti, P.P. Camanho, J. Xavier, C.G. Dávila, A.T. Marques, Measurement of resistance curves in the longitudinal failure of composites using digital image correlation, Compos. Sci. Technol. 70 (13) (2010) 1986–1993.
[42] Scilab (Version 6.0.1). Available online: http://www.scilab.org/download/6.0.1.